Use of geostatistical models to evaluate landscape and stream network controls on post-fire stream nitrate concentrations

Allison E. Rhea[1], Tim Covino[1], Charles C. Rhoades[2], and Alexander C. Brooks[1]

[1]Colorado State University
[2]USDA Forest Service Rocky Mountain Research Station

June 11, 2022

Abstract

Forested watersheds provide many ecosystem services that have become increasingly threatened by wildfire. Stream nitrate (NO_3^-) concentrations often increase following wildfire and can remain elevated for decades. We investigated the drivers of persistent elevated stream NO_3^- in nine watersheds that were burned to varying degrees 16 years prior by the Hayman fire, Colorado, USA. We evaluated the ability of multiple linear regression and spatial stream network modeling approaches to predict observed concentrations of the biologically active solute NO_3^- and the conservative solute sodium (Na^+). Specifically, we quantified the degree to which landscape and stream network characteristics predict stream solute concentrations. No landscape variables were strong predictors of stream Na^+. Rather, stream Na^+ variability was largely attributed to flow-connected spatial autocorrelation, indicating that downstream hydrologic transport was the primary driver of spatially distributed Na^+ concentrations. In contrast, vegetation cover, measured as mean normalized differenced moisture index (NDMI), was the strongest predictor of spatially distributed stream NO_3^- concentrations. Furthermore, stream NO_3^- concentrations had weak flow-connected spatial autocorrelation and high spatial variability. This pattern is likely the result of spatially heterogeneous wildfire behavior that leaves intact forest patches interspersed with high burn severity patches that are dominated by shrubs and grasses. Post-fire vegetation also interacts with watershed structure to influence stream NO_3^- patterns. For example, severely burned convergent hillslopes in headwaters positions were associated with the highest stream NO_3^- concentrations due to the high proportional influence of hillslope water in these locations. Our findings suggest that reforestation is critical for the recovery of stream NO_3^- concentrations to pre-fire levels and targeted planting in severely burned convergent hillslopes in headwater positions will likely have a large impact on stream NO_3^- concentrations.

Use of geostatistical models to evaluate landscape and stream network controls on post-fire stream nitrate concentrations

Allison E. Rhea[1*], Timothy P. Covino[1], Charles C. Rhoades[2], and Alexander C. Brooks[1]

[1]Colorado State University, Department of Ecosystem Science and Sustainability

[2]US Forest Service, Rocky Mountain Research Station

*Corresponding author: Allison Rhea (Allison.Rhea@colostate.edu)

Abstract

Forested watersheds provide many ecosystem services that have become increasingly threatened by wildfire. Stream nitrate (NO_3^-) concentrations often increase following wildfire and can remain elevated for decades. We investigated the drivers of persistent elevated stream NO_3^- in nine watersheds that were burned to varying degrees 16 years prior by the Hayman fire, Colorado, USA. We evaluated the ability of multiple linear regression and spatial stream network modeling approaches to predict observed concentrations of the biologically active solute $NO_3^-$and the conservative solute sodium (Na^+). Specifically, we quantified the degree to which landscape and stream network characteristics predict stream solute concentrations. No landscape variables were strong predictors of stream Na^+. Rather, stream Na^+ variability was largely attributed to flow-connected spatial autocorrelation, indicating that downstream hydrologic transport was the primary driver of spatially distributed Na^+ concentrations. In contrast, vegetation cover, measured as mean normalized differenced moisture index (NDMI), was the strongest predictor of spatially distributed stream NO_3^-concentrations. Furthermore, stream NO_3^- concentrations had weak flow-connected spatial autocorrelation and high spatial variability. This pattern is likely the result of spatially heterogeneous wildfire behavior that leaves intact forest patches interspersed with high burn severity patches that are dominated by shrubs and grasses. Post-fire vegetation also interacts with watershed structure to influence stream NO_3^- patterns. For example, severely burned convergent hillslopes in headwaters positions were associated with the highest stream NO_3^-concentrations due to the high proportional influence of hillslope water in these locations. Our findings suggest that reforestation is critical for the recovery of stream NO_3^-concentrations to pre-fire levels and targeted planting in severely burned convergent hillslopes in headwater positions will likely have a large impact on stream NO_3^-concentrations.

1 Introduction

Wildfires are a natural part of many forested ecosystems, but the frequency and severity of wildfires has been increasing across the Western US (Abatzoglou et al., 2017; Westerling, 2016). Elevated wildfire activity can threaten the function of critical forested watersheds that supply clean water to much of the Western US (Brown et al., 2008). Nitrogen (N) typically limits plant growth so N export often indicates ecosystem disturbance and shifts in nutrient supply and demand (Chapin et al., 2011). Short-term (<5 years) increases in stream nitrate (NO_3^-) have been documented following wildfires across the Western US (Rust et al., 2018; Smith et al., 2011) due to elevated soil N mineralization and leaching (Smithwick et al., 2009; Turner et al., 2007; Wan et al., 2001). In some cases, stream NO_3^- can remain elevated for decades and has been shown to decrease with post-fire vegetation cover (Rhoades et al., 2019; Rust et al., 2019) and increase with burn extent (Rhoades et al., 2019). These results suggest that a lack of vegetation recovery is likely a dominant driver of persistent post-fire NO_3^- export, but this relationship remains poorly understood.

The interaction of vegetation cover, watershed structure, and stream network geometry regulates watershed solute export (Abbott et al., 2021; Covino et al., 2021; Creed & Beall, 2009; Likens & Bormann, 1974; Lovett et al., 2002; Shogren et al., 2021; Zarnetske et al., 2018). Watershed structure is the spatial arrangement of divergent and convergent hillslopes across the landscape (Baiamonte & Singh, 2016; Jencso et al., 2010). Divergent hillslopes are convex and contribute little flow to the stream, whereas convergent hillslopes concentrate hydrologic flowpaths and contribute large inputs to channel networks (Detty & McGuire, 2010). In headwater positions, water and solutes are primarily derived from shallow groundwater contributions from adjacent hillslopes (Covino et al., 2021; Gomi et al., 2002; Likens & Bormann, 1974) whereas upstream sources increasingly dominate water composition in lower network positions (Vannote et al., 1980). Therefore, headwaters are particularly sensitive to disturbance in the surrounding uplands (Lowe & Likens, 2005) and contributions to the stream in these locations have the potential to exert strong control on downstream solute concentrations (Abbott et al., 2018; Alexander et al., 2007; Wohl, 2017).

To better understand the spatial patterns in post-fire water chemistry, we consider both conservative and reactive solutes. Conservative solutes, such as sodium (Na^+), have low biological demand (Dingman, 2015; Stream Solute Workshop, 1990) and thus are primarily driven by physical transport processes (Webster & Valett, 2006) and watershed geophysical properties (Brennan et al., 2016; French et al., 2020; McGuire et al., 2014). In contrast, biologically active solutes such as NO_3^- are controlled by interactions between hydrologic transport and biological uptake (Bernhardt et al., 2003, 2005). In particular, forest cover can be a primary control on NO_3^- export at the watershed scale (Bormann & Likens, 1967; Likens et al., 1970).

Statistical models can be used to partition the spatial variance in stream Na^+ and NO_3^-among landscape (i.e., topographic, vegetation, and fire predictors) and stream network (i.e., flow-connected distance) characteristics. Multiple linear regression (MLR) modeling can be used to determine the relative influence of specific landscape characteristics on spatially distributed solute concentrations (Cho & Lee, 2018; McManus et al., 2020), but this approach assumes independence of sampling locations. Geostatistical modeling approaches, such as spatial stream network (SSN) models, are better suited to differentiate landscape from stream network attributes since they account for spatial autocorrelation of flow-connected samples and the dendritic and unidirectional nature of stream networks (Ver Hoef et al., 2014; Isaak et al., 2014; Peterson & Ver Hoef, 2010). We paired spatially distributed water chemistry sampling with terrain analysis and vegetation and fire mapping to address the following objectives: 1) examine the degree to which topographic, vegetation, and fire variables predict stream Na^+ and NO_3^- across spatial scales and 2) evaluate the performance of MLR and SSN models in predicting stream solute concentrations. To our knowledge, this study is the first to use geostatistics to investigate the drivers of elevated post-fire stream NO_3^-.

2 Materials and Methods

2.1 Site description

In 2002, the Hayman Fire burned more than 554 km^2 of ponderosa pine (*Pinus ponderosa*) and Douglas-Fir (*Pseudotsuga menziesii*) forest in the Pike San Isabel National Forest (Graham, 2003) (Figure 1). This was one of the largest wildfires in Colorado's recorded history and 35% of the fire burned at high severity (Robichaud et al., 2003). The fire burned the contributing area of Cheesman Reservoir, a primary drinking water supply to the city of Denver (Graham, 2003). In combination, the 2002 Hayman and 1996 Buffalo Creek fires cost Denver's public water utility tens of millions of dollars on water quality treatment, sediment and debris removal, and reclamation (Hall, 2017). Watersheds within the Hayman Fire burn perimeter receive an annual average of 40 cm of precipitation (WRCC, 2021) and 60-75% of that comes from summer monsoonal rains (Wilson et al., 2018). Mean elevation within the fire perimeter is 2462 m which is within the intermittent snow zone that does not maintain snow cover throughout the winter (Richer et al., 2013). The parent material underlying our study area is dominated by Pike's Peak Formation granite (Ruleman et al., 2011) which weathers to form coarse, sandy loam soils (Cipra et al., 2003). Ambient Na^+ concentrations are relatively low in granitic basins in our study area. There were no reported post-fire increases in stream Na^+ and measured post-fire increases in other geochemical ions (i.e., calcium, acid neutralizing capacity, and conductivity) recovered to pre-fire levels 2 years after the Hayman Fire (Rhoades et al., 2011).

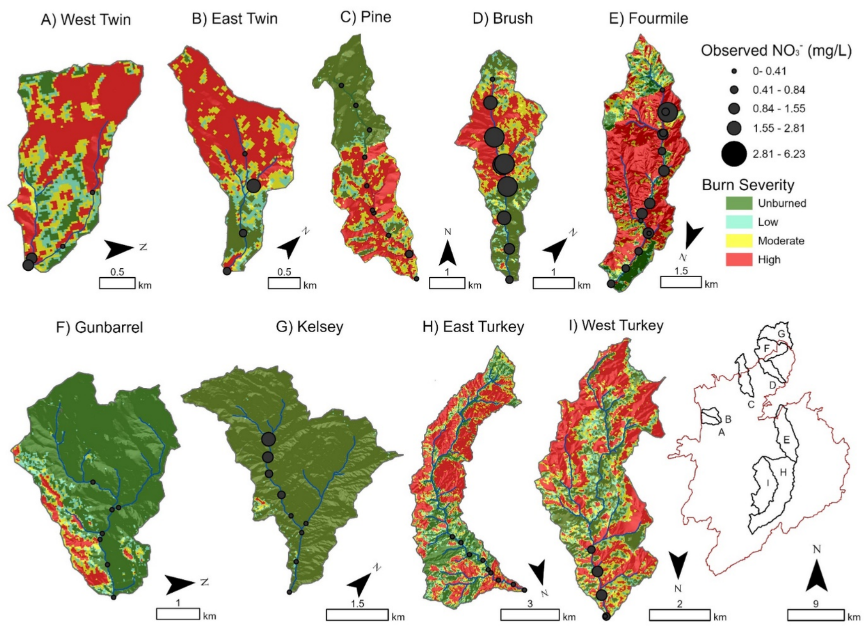

Figure 1: Sampling locations within the study watersheds affected by the 2002 Hayman Fire, Colorado, USA. Water chemistry samples (n=71) were collected in June 2018 and the symbol size at each sampling point increases with stream NO_3^-concentration.

Our nine study watersheds ranged in size from 3.2 to 35.4 km^2, slope from 17-38%, and elevation from 2284-2694 m (Table 1). At the time of our sampling, 16 years after the fire, mean normalized differenced moisture index (NDMI) was the lowest in Brush (-0.13) and highest in Gunbarrel (-0.02) where burn extents were 71 and 18% respectively (Tables 1-2). Burn extent varied from 1-90% across the watersheds, but seven of them had more than half of their contributing area burned and 36-64% of that burned at high severity (Table 2). Patch density was high which is consistent with a mixture of fire severity classes. High severity patches, defined by complete canopy consumption, generally had the largest patch size and radius (Table 2), suggesting that post-fire pine reestablishment may be limited in high severity areas (Chambers et al., 2016).

Table 1: Physical characteristics and solute concentrations of each study watershed for samples collected in June 2018.

	Physical Characteristics	**Physical Characteristics**	**Physical Characteristics**	**Physical Chara**
Watershed	**Outlet UAA (km²)**	**Mean Slope (%)**	**Mean Elev. (m)**	**Mean NDMI ( )**
Fourmile	18.8	26	2441	-0.11
East Twin	3.2	30	2640	-0.06
West Twin	3.3	38	2694	-0.05
West Turkey	22	25	2523	-0.08
East Turkey	35.4	17	2571	-0.08
Brush	6.1	28	2277	-0.13
Pine	9.3	35	2516	-0.06
Gunbarrel	12.3	27	2361	-0.02
Kelsey	12.1	22	2284	-0.04

Note: UAA is upslope accumulated area, NDMI is the average normalized differenced moisture index in June 2018, and cv is the coefficient of variation.

Table 2: Burn metrics by severity for each study watershed. These metrics represent immediate fire impacts by differencing one pre-fire (8/24/2001) and one post-fire (8/14/2003) Landsat image and severity is classified according to MTBS thresholds (Eidenshink et al., 2009).

Watershed	**Burn Extent**	**Burn Extent**	**Burn Extent**	**Mean Patch Size / Mean Patch Radius**	**Mean P**
	Low (%)	**Moderate (%)**	**High (%)**	**Unburned (ha / m)**	**Low (ha / m**
Fourmile	8	17	64	2 / 29	1 / 22
East Twin	10	22	57	1 / 21	1 / 23
West Twin	12	26	51	1 / 39	1 / 27
West Turkey	13	20	46	3 / 41	0 / 23
East Turkey	12	17	45	4 / 37	0 / 23
Brush	11	23	38	4 / 40	0 / 23
Pine	7	16	36	8 / 43	0 / 20
Gunbarrel	6	6	6	73 / 130	0 / 20
Kelsey	1	0	0	597 / 758	0 / 8

2.2 Stream sampling

To capture a gradient of disturbance and quantify the spatial variability of post-fire stream Na^+ and NO_3^-, we sampled stream water roughly every 800 meters along the mainstems of our study watersheds (Figure 1). This distance was selected to ensure a consistent sampling interval that maximized the number of samples collected per watershed but would allow us to complete watershed sampling within one day. Low-flow conditions were stable and there were no precipitation events during our sampling period (6/1/2018-6/7/2018). Previous research at the Hayman Fire demonstrated that patterns of elevated stream NO_3^- in severely burned watersheds persist across flow conditions (Rhoades et al., 2019) so our June sampling date should be broadly representative. All stream samples from a given watershed were collected within a single day in pre-washed 1 L high-density polyethylene bottles moving in the upstream direction. Samples were immediately filtered with 0.45 µm polyvinyl diethylene filters (MilliporeSigma, Burlington, MA) and analyzed for concentrations of stream Na^+ and NO_3^- using ion chromatography (Dionex ICS-3000, Waltham, MA and Waters 580, Sunnyvale, CA). Detection limits for both Na^+ and NO_3^- were 0.01 mg/L; any concentrations below that were replaced with $\frac{1}{2}$ the detection limit.

2.3 Geospatial analysis

We conducted a terrain analysis to characterize the underlying watershed structure. First, flow direction was derived from a 10-m digital elevation model (DEM) (U.S. Geological Survey, 2018) using the multiple triangular flow direction algorithm (Seibert & McGlynn, 2007). Watershed contributing areas were delineated and upslope accumulated area (UAA) was calculated for all sampling points (0.32 – 35.4 km^2) using the openSTARS package (Peterson & Ver Hoef, 2014) in R Studio. We summarized topographic, vegetation, and fire variables as means and proportional extents within the contributing areas for each sampling location (Table 3).

Table 3: Watershed predictor variables that were summarized for the contributing area to each sampling point. Pearson correlation coefficients were calculated between each predictor variable and Na^+ or NO_3^-. Vegetation metrics represent current conditions (i.e., June 2018) whereas fire metrics represent immediate post-fire condition (i.e., August 2003). Variables marked with a x were removed prior to linear mixed model selection due to strong correlation (>0.90) with another predictor variable. Coefficients depicted in grey

identify variables removed during linear mixed model selection; those in black were retained for subsequent modeling.

	Variable	Summary Statistic	Data Source	Correlation Coeffic
				Na^+
Topographic	Watershed area	value at sampling point	Whitebox flow accumulation tool	0.12
	Slope	watershed mean	Whitebox slope tool	0.27
	Elevation	watershed mean	10-m digital elevation model	-0.23
	Riparian extent	% of watershed area	Whitebox elevation above stream tool	0.24
	TWI	watershed mean	Whitebox twi tool	-0.33
Vegetation	Tree cover	watershed mean	Rangeland Analysis Platform	0.15
	Shrub cover	watershed mean	Rangeland Analysis Platform	-0.24
	Bare x	watershed mean	Rangeland Analysis Platform	-0.12
	NDMI	watershed mean	Climate Engine	0.09
	NDVI x	watershed mean	Climate Engine	0.05
	EVI x	watershed mean	Climate Engine	-0.02
Fire	Burn extent	% of watershed area	MTBS	-0.24
	dNBR x	watershed mean	MTBS	-0.26

Note: TWI: topographic wetness index, Bare is bare ground cover; NDMI: normalized differenced moisture index, NDVI: normalized differenced vegetation index, EVI: enhanced vegetation index, dNBR: differenced normalized burn ratio, and MTBS: monitoring trends in burn severity database.

Topographic metrics included watershed area, mean slope, mean elevation, riparian extent, and mean topographic wetness index (TWI) (Table 3). Slope, elevation, and TWI were derived from the 10-m DEM using Whitebox tools (Lindsay, 2020; Wu, 2021) and summarized as watershed means. We used a physical definition of the riparian corridor that included pixels <2 m above the stream surface elevation (*sensu* Jencso et al., 2010) and calculated riparian extent as the total riparian corridor area divided by UAA of each sampling point. This approach differs from an earlier estimate of the extent of riparian vegetation in these watersheds (Rhoades et al., 2019).

We characterized vegetation condition using normalized differenced vegetation index (NDVI), normalized differenced moisture index (NDMI), and enhanced vegetation index (EVI). We obtained mean June 2018 vegetation indices from Landsat using Climate Engine (Huntington et al., 2017) to match the vegetation characterization with the timing of our stream sampling. We also included 2018 fractional land cover estimates derived from satellite imagery that was extensively calibrated across the Western US and estimated the proportion of each Landsat pixel covered by trees, shrubs, and bare ground (Allred et al., 2021).

Mean differenced normalized burn ratio (dNBR, a measure of burn severity) and burn extent were calculated for the area contributing to each sampling point. These fire metrics represent immediate post-fire impacts by differencing one pre-fire (8/24/2001) and one post-fire (8/14/2003) Landsat image. dNBR was then classified into categorical burn severity as follows: -150-140 unburned; 140-211 low severity; 211-350 moderate severity, 350-953 high severity (Eidenshink et al., 2009). Low severity fire tends to leave tree canopies largely unaltered whereas high severity fire typically causes complete consumption of surface organic matter and canopy foliage (Parsons et al., 2010). Wildfire severity varies spatially across topographic, vegetation (i.e., fuel composition, arrangement, condition), and weather gradients (Taylor et al., 2021) which creates mosaics of post-fire vegetation structure and composition that vary at scales finer than mapped severity patches (Lentile et al., 2007). To characterize the spatial burn patterning of each watershed, we calculated burn extent, patch size, patch radius, and patch density by severity (Table 2). Burn extent reflects the proportion of watershed area that was burned by each severity class. All patch metrics were calculated with the landscape metrics package (Hesselbarth et al., 2019) in R Studio which defines contiguous cells belonging to the same burn severity class. For each watershed, we determined patch area and calculated patch radius as the mean distance from each cell in a patch to its centroid, and patch density as the number of patches divided by watershed UAA.

2.4 Statistical modeling

We used statistical models to evaluate the degree to which topographic, vegetation, and fire variables and flow-connected distance control post-fire stream water chemistry – specifically, concentrations of Na^+ and NO_3^-. Concentration data were log-transformed to improve normality and a correlation analysis removed redundant predictor variables with a correlation >0.90 (Figure 2, Table 2). To identify the top-performing Na^+ and NO_3^- models, we went through a two-step model selection process (sensu McManus et al., 2020; Rodríguez-González et al., 2019). First, we identified which landscape characteristics best predicted stream Na^+ and NO_3^- using linear mixed model selection (Supplemental Table 1). The Na^+ and NO_3^- models with the lowest maximum likelihood estimate of Akaike's Information Criteria (AIC) then progressed to the second phase of model selection where we compared spatial autocorrelation approaches. We initially ran multiple linear regression (MLR) models which use landscape characteristics to predict observed water chemistry at each sampling location. The predictor variables are spatially explicit given that they characterize the area contributing to a specific sampling point, but MLR models assume independence between stream water samples. We then compared MLR models to spatial stream network (SSN) models that jointly consider landscape and stream network characteristics. This approach captures spatial effects beyond those directly attributable to predictor variables by accounting for flow-connection (Isaak et al., 2014). MLR and SSN model performance was compared through iterative leave-one-out cross-validation. Observations at sampling points were removed one at a time and the model was used to predict each of the removed values along with the prediction standard error (Ver Hoef & Peterson, 2020). The model with the lowest AIC and root mean square prediction error (RMSPE) was selected for subsequent analyses.

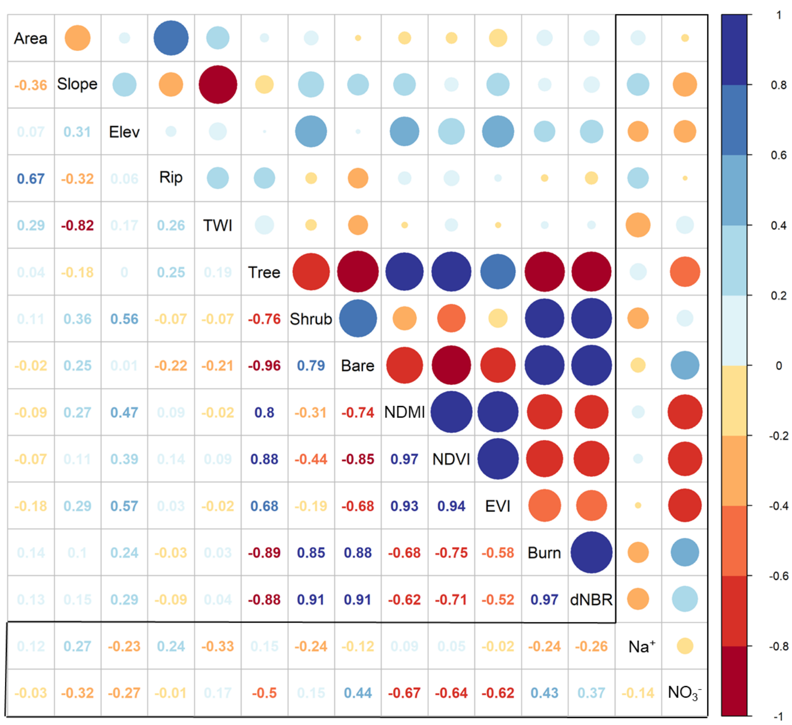

Figure 2 : Pearson correlation matrix between all potential predictor and response variables. The black box highlights correlations between the predictor variables and stream Na^+ and NO_3^-, both of which were

log-transformed. Everything beyond the black box represents correlations among predictor variables.

Note: Area is watershed area, Slope is mean watershed slope, Elev is mean watershed elevation; Rip is riparian extent, TWI is mean topographic wetness index, Tree is mean tree cover (%), Shrub is mean shrub cover (%), Bare is mean bare ground cover (%), NDMI is mean normalized differenced moisture index, NDVI is mean normalized vegetation index, EVI is mean enhanced vegetation index, Burn is burn extent (%), dNBR is mean differenced normalized burn ratio, and both stream NO_3^- and stream Na^+ concentrations are log-transformed (mg/L).

To build SSN models, stream sampling locations were incorporated into a landscape network (LSN) to characterize network geometry (Peterson & Ver Hoef, 2014) using the openSTARS package (Kattwinkel & Szöcs, 2020). The additive function quantified the proportional influence of each stream segment (Ver Hoef & Peterson, 2020) and calculated distance matrices between all sampling points. We used a tail-up autocovariance structure to restrict our modeling to flow-connected distance, which is only measured between points with an upstream-to-downstream connection (Isaak et al., 2014; Peterson & Ver Hoef, 2010). This distance metric is better suited for stream network studies than straight-line Euclidean distance because it characterizes downstream transport and longitudinal connectivity of dissolved solutes (Peterson & Ver Hoef, 2010). We then modeled an empirical semivariogram and derived 3 associated parameters – the nugget, sill, and range. Empirical semivariograms quantify the variation between samples (i.e., stream Na^+ or NO_3^- concentrations) as a function of distance between sampling points (Ganio et al., 2005). Positive autocorrelation occurs when semivariance is smaller (i.e., measurements are more similar) near the origin and increases at greater lag distances. In some cases, the semivariogram will reach an inflection point at a given lag distance ('range') where semivariance begins to flatten out ('sill'). Samples are considered uncorrelated at distances greater than the range and the sill represents the dissimilarity of the uncorrelated data (Isaak et al., 2014). The nugget describes spatial variation at scales smaller than the minimum sampling interval (i.e., [?]52 m in our study).

2.5 Longitudinal patterns across two watersheds with inverse burn patterns

Finally, we used kriging to interpolate stream NO_3^- concentrations along the mainstems of two paired watersheds and compared spatial NO_3^- patterns to continuous measures (i.e., every 10 m) of hydrologic inputs and the vegetation condition of those inputs. These two watersheds had similar contributing areas (6.1 and 9.3 km^2, Table 1) and were extensively burned (i.e., >50% of UAA burned). For both watersheds, patch density was high and fire severity was mixed equally among burn severity classes (Table 2). However, the headwaters were severely burned in Brush Creek and unburned in Pine Creek (Figure 1). We distributed 3,000 equally spaced prediction points along the geomorphic channel networks of each watershed, delineated the contributing area of each prediction point, and calculated topographic, vegetation, and fire predictor variables (see section 2.3). We also calculated the flow-connected distance between all observed and prediction locations. The NO_3^- SSN model then predicted NO_3^- concentration and standard error at each location based on both landscape characteristics (i.e., watershed area, riparian extent, mean TWI, and mean NDMI) and flow-connected distance. We then calculated the relative lateral input (LI) as the incremental downstream increase in contributing area relative to the total contributing area (i.e., Relative LI $=\frac{(\mathrm{UAA}_{\mathrm{cell}(n)}\ \ \mathrm{UAA}_{\mathrm{cell}(n-1)})}{\mathrm{UAA}_{cell(n)}}$). Because stream discharge scales with contributing area (Bergstrom et al., 2016), this metric reflects the contribution of hillslope water relative to mainstem flow. Finally, mean NDMI was calculated for the discrete lateral input (LI) contributing to each 10-m stream cell using the same June 2018 NDMI image described in section 2.3. We also resampled the paired watersheds in June of 2019 at a 300 m resolution to assess the accuracy of our NO_3^- SSN predictions with observed values.

3 Results

3.1 Stream Na^+ and NO_3^-concentrations

Observed stream Na^+ concentrations ranged from 3.9-13.1 mg/L (Supplemental Figure 1), with an average concentration of 7.3 mg/L which is similar to the pre-fire average of 6.1 mg/L reported in these granitic basins (Rhoades et al., 2011). Kelsey had the highest and Brush had the lowest mean stream Na^+ concentration whereas Brush had the highest and West Turkey had the lowest coefficient of variation (Table 1). Observed stream NO_3^- concentrations varied by three orders of magnitude (0.005 – 6.2 mg/L) and average stream NO_3^- concentration was 0.91 mg/L which is five times greater than pre-fire concentrations (0.18 mg/L) (Rhoades et al., 2019). Brush watershed had the highest (3.06 mg/L) and Gunbarrel the lowest (0.16 mg/L) mean NO_3^-concentration whereas Fourmile had the greatest and West Turkey the lowest coefficient of variation (Table 1). The coefficient of variation was consistently higher for stream NO_3^- (Table 1) indicating greater within-watershed variability in stream NO_3^- compared to Na^+.

3.2 Landscape controls on Na^+ and NO_3^-

Topographic, vegetation, and fire predictor variables were weakly correlated ([?]0.33) with log[Na^+] (Table 3). Linear mixed model selection identified watershed area, slope, riparian extent, TWI, and tree and shrub cover as the best predictors of log[Na^+] (Supplemental Table 1). Stream Na^+ was related positively to watershed area, slope, riparian extent, and tree cover, and negatively to TWI, and shrub cover (Figure 2). All watershed predictors were significant in the Na^+ MLR model and together explained 54.4% of the variance in log[Na^+] (Table 4). Predictor variables explained 45% of the variance in log[Na^+] in the Na^+ SSN model and all predictors except watershed area were significant (Table 4).

Table 4: Summary of spatial stream network (SSN) and multiple linear regression (MLR) models that predict log-transformed stream Na^+ and NO_3^-concentrations. Parameter estimates represent the regression coefficient, which is the change in the response variable based on a 1-unit change in the predictor variable while holding all other variables constant. Statistical significance of predictor variables is denoted with symbols *=0.05, **=0.01, ***=0.001. Variance decomposition assigns variance in Na^+ or NO_3^- to watershed predictor variables, flow-connected autocorrelation, and unexplained variance. MLR models do not account for flow-connected autocovariance. Model performance metrics come from iterative leave-on-out cross-validation.

		Na^+ Models	**Na^+ Models**	**NO_3^- Models**	**NO_3^- Models**
		SSN	**MLR**	**SSN**	**MLR**
Parameter Estimates	Watershed Area	0.008	0.012 **	-0.03	-0.04 *
	Slope	0.090 ***	0.104 ***	-	-
	Elevation	-	-	-	-
	Riparian Extent	0.100 **	0.106 ***	0.32	0.29
	TWI	0.651 *	0.813 ***	1.33 *	0.91 *
	Tree cover	-0.02 ***	-0.018 ***	-	-
	Shrub cover	-0.115 ***	-0.111 ***	-	-
	NDMI	-	-	-17.64 ***	-17.37 ***
	Burn extent	-	-	-	-
Variance Components (%)	Predictor variables	45.0	54.4	36.0	51.4
	Flow-connected distance	53.1	-	41.5	-
	Total explained	98.1	54.4	77.5	51.4
	Unexplained	1.9	45.6	22.5	48.6
Model Performance	AIC	-55.35	-34.29	210	212
	RMSPE	0.165	0.205	1.00	1.07

Note: TWI is topographic wetness index, NDMI is normalized difference moisture index, AIC is Akaike's information criteria, and RMSPE is root mean square prediction error.

Fire and vegetation variables generally had stronger correlations (0.15-0.67) with log[NO_3^-] than topographic variables (0.03 – 0.32) (Table 3). Linear mixed model selection identified watershed area, riparian extent, TWI, and NDMI as the best predictors of log[NO_3^-] (Supplemental Table 1). Stream $NO_3^-$was positively related to riparian extent and TWI, but negatively related to watershed area and NDMI (Figure 2). Mean NDMI had the strongest correlation with log[NO_3^-] (Figure 2). In the NO_3^- MLR model, the selected predictor variables, with the exception of riparian extent, were significant and accounted for 51.4% of the variance in log[NO_3^-] (Table 4). In the NO_3^- SSN model, TWI and NDMI were the only significant predictor variables and the predictors explained 36% of variation in log[NO_3^-] (Table 4).

Topographic variables had weak correlations (<0.32) with both stream Na^+ and NO_3^-(Table 3). Vegetation predictors generally had much stronger correlations with NO_3^- compared to Na^+, with the exception of shrub cover (Table 3). Burn variables had slightly higher correlations with NO_3^- compared to Na^+(Table 3). All predictor variables that were selected through linear mixed model selection were weakly correlated with water chemistry (<0.33) (Supplemental Figure 2). The one exception was a strong inverse relationship between mean NDMI and stream NO_3^- which had a correlation coefficient of -0.67 (Supplemental Figure 2).

3.3 Stream network controls on Na^+ and NO_3^-

In the Na^+ SSN model, a majority of variation (53.1%) in log[Na^+] was explained by flow-connected autocorrelation (Table 4). Na^+ exhibited strong positive autocorrelation where semivariance was low at short lag distances, but increased with distance (Figure 3). When flow-connected autocovariance was modeled with a spherical fit, Na^+had a nugget of 0.001, sill of 0.029, and range of 3700 m (Figure 3). The low nugget suggests that our sampling adequately captured variability at small spatial scales and that there is relatively little unexplained variation. The low sill reflects the low overall variance in streamwater Na^+ concentrations. The range indicates that samples that are > 3700 m apart are no longer correlated.

In the NO_3^- SSN model, flow-connected autocorrelation explained 41.5% of variation in log[NO_3^-] (Table 4). Stream NO_3^- had high semivariance across all flow-connected distances, though semivariance peaked at intermediate lag distances (1000-5000 m) (Figure 3). When flow-connected autocovariance was modeled with an exponential fit, NO_3^- had a nugget of 0.385, sill of 0.708, and range of 8800 m which is equal to our maximum sampling distance (Figure 3). The large nugget and sill values are consistent with the substantial unexplained variance and high overall variance in stream NO_3^- concentrations. The lowest semivariance in NO_3^- is still greater than the maximum Na^+ semivariance (Figure 3).

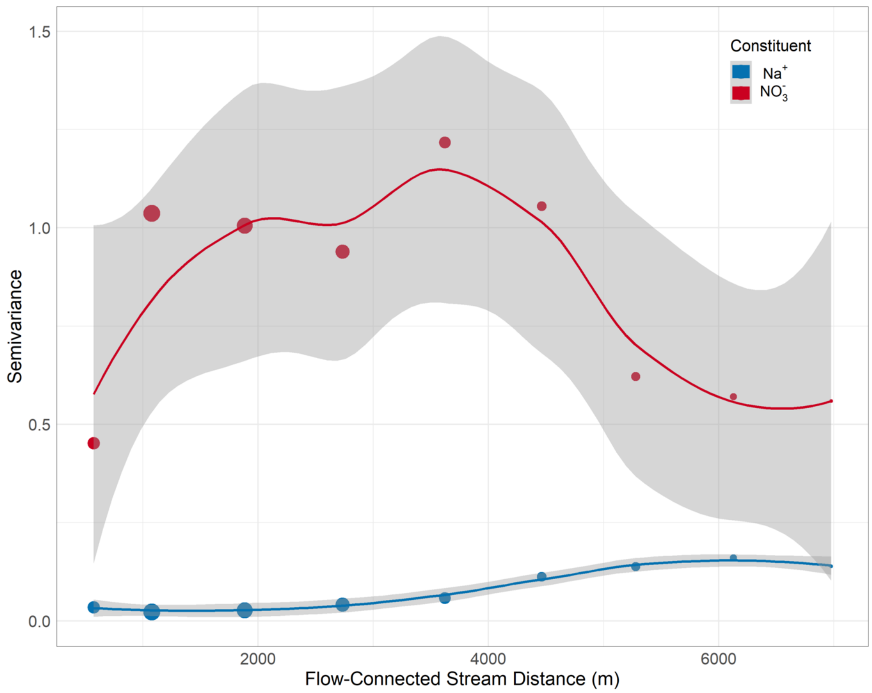

Figure 3: Empirical semivariograms of log-transformed stream Na^+ (blue) and NO_3^-(red) based on the flow-connected distance between sampling points. Symbol sizes are proportional to the number of data pairs included in each bin. The grey shaded region represents the 95% confidence interval from a local polynomial regression of each semivariogram. Semivariograms show evidence of strong positive autocorrelation in Na^+ (blue) and weak spatial autocorrelation in NO_3^- (red).

3.4 Statistical model performance

The SSN model improved Na^+ predictions relative to the MLR model, as indicated by lower AIC and RMSPE values (Table 4). Leave one-out-cross validation demonstrated that SSN predictions were closer to observed values (Figure 4A) and prediction standard errors were lower (Figure 4C) in the Na^+ SSN model compared to the Na^+ MLR model. In the Na^+ SSN model, predictor variables explained 45% of the variance in log[Na^+], flow-connected autocovariance explained 53.1% and only 1.9% was left unexplained (Table 4).

The NO_3^- SSN model also had a lower AIC value and RMSPE relative to the NO_3^- MLR model (Table 4). SSN predictions were closer to the observed values (Figure 4B) and prediction standard error was lower (Figure 4D) in the NO_3^- SSN model than the MLR model. In the NO_3^- SSN model, predictor variables (36%) and flow-connected autocovariance (41.5%) explained a majority of the variation in log[NO_3^-], leaving 22.5% unexplained (Table 4). Based on NO_3^-SSN model, 81% of the predicted stream NO3 concentrations that fell within the fire perimeter exceeded the pre-fire mean concentrations of 0.18 mg/L (Rhoades et al., 2011, Supplemental Figure 3).

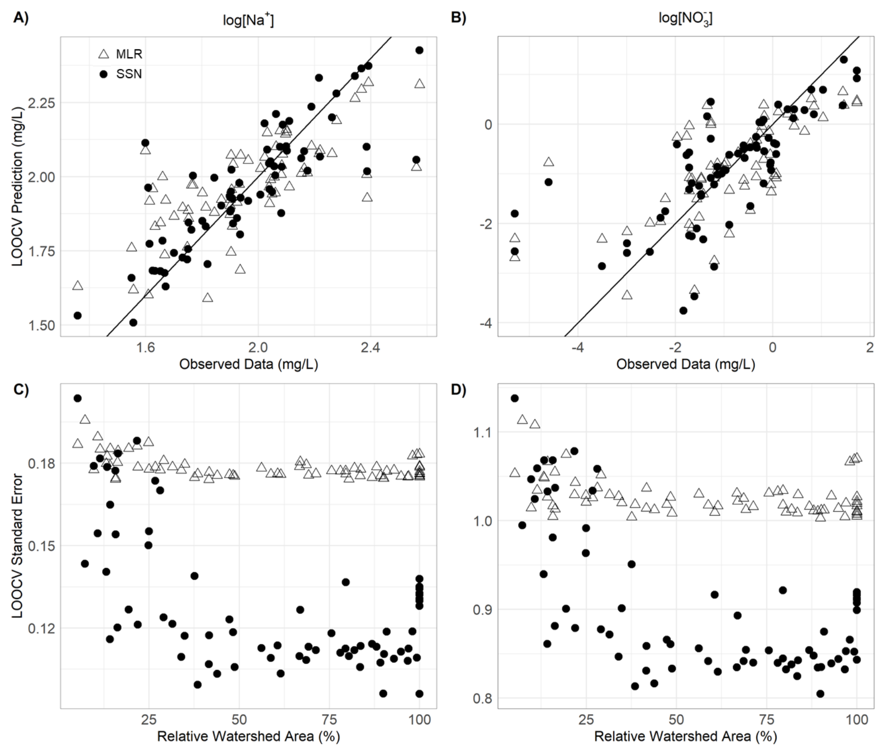

Figure 4 : Leave-one-out cross validation to assess A, C) Na^+ and B, D) NO_3^-model performance. A-B) Model predictions are plotted against observed values for both MLR (open triangles) and SSN (black circles) models. C-D) Prediction standard error is plotted against relative watershed area, with headwater positions on the left side of the plot and lower watershed positions on the right side.

3.5 Longitudinal patterns across two watersheds with inverse burn patterns

The two paired watersheds with inverse burn patterns exhibited distinct patterns in stream NO_3^- concentration. 72% of Brush watershed was burned and most of the burn occurred in the upper half of the watershed (Figure 5A). Mean NDMI was generally low throughout Brush, but was inversely related to burn extent (Figure 5C). Stream NO_3^- concentrations spanned a 4.6 mg/L range throughout Brush Creek. The minimum concentration (0.4 mg/L) occurred at the upper most sampling location and the highest observed concentration (5.0 mg/L) occurred nearby within the upper watershed (Figure 5E). Nitrate generally declined in the lower half of the watershed and reached 0.9 mg/L at the lowest sampling location. Conversely, the majority of the burned area in Pine Creek occurred in the lower watershed (Figure 5B). Burn extent was again inversely related to mean catchment NDMI, but NDMI remained relatively high throughout (Figure 5D). Pine stream NO_3^-concentration increased gradually downstream from below detection levels in the headwaters to 0.3 mg/L at the outlet (Figure 5F). Maximum and mean stream NO_3^- concentrations was 14- and 17-times higher in Brush than Pine. Our NO_3^- SSN model predictions agreed with measured stream NO_3^- concentrations during our 2019 sampling (Supplemental Figure 4).

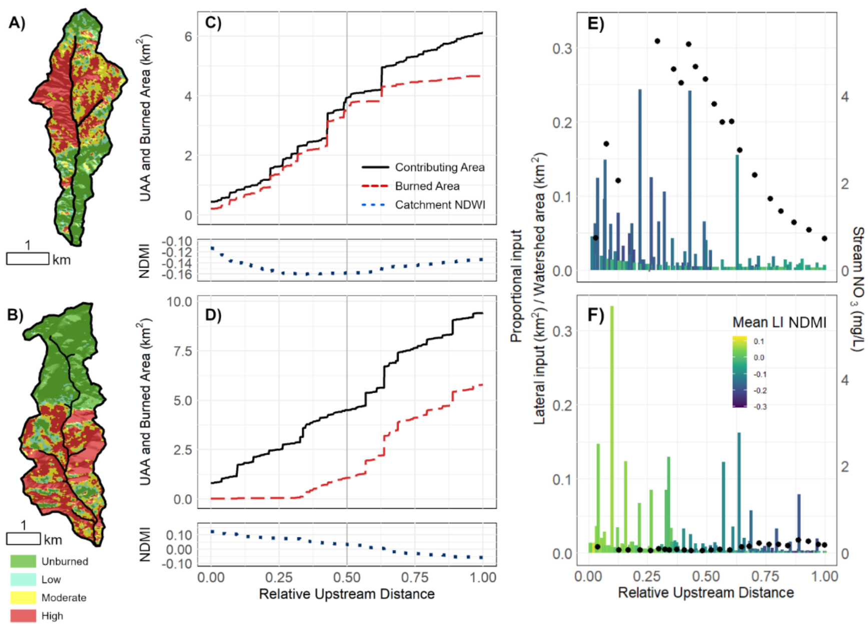

Figure 5 : Spatial arrangement of burn severity in A) Brush Creek which was 71% burned with most high severity fire occurring in the upper watershed and B) Pine Creek which was 59% burned with most high severity fire occurring in the lower watershed. Distribution of cumulative upslope accumulated area (black solid lines), cumulative burned area (red dashed lines), and mean catchment NDMI (blue dotted lines) for C) Brush and D) Pine. Upstream distance was relativized between 0 and 1 in all plots, with headwaters on the left and outlet on the right, to allow for comparisons between watersheds. The vertical grey line denotes the mid-point of the watershed. Distribution of relative lateral inputs with upstream distance for E) Brush and F) Pine where bars are colored according the mean NDMI of each discrete lateral input. Stream NO_3^- concentrations predicted from the NO_3^- SSN model (black circles) are compared for both E) Brush and F) Pine.

4 Discussion

4.1 Modeling streamwater chemistry in burned watersheds

Multiple lines of evidence indicated that stream NO_3^- concentrations had greater spatial variability and weaker spatial structuring relative to Na^+. First, semivariance was greater for stream NO_3^- than Na^+ across all flow-connected distances (Figure 3) which suggests higher variability in stream NO_3^-concentrations across all measured scales (Isaak et al., 2014). Secondly, the nugget effect was orders of magnitude greater for stream NO_3^- than Na^+ (0.385 and 0.001 respectively) which indicates unmeasured fine-scale variability in stream NO_3^-concentrations (Cooper et al., 1997). Finally, Na^+semivariance increased with lag distance and stabilized around 3,700 m (Figure 3). This strong positive autocorrelation indicates that downstream hydrologic transport was the primary driver of spatially distributed Na^+ concentrations. In contrast, the empirical semivariogram for NO_3^-exhibited irregular trends in semivariance that did not stabilize across the measured range in spatial scales (Figure 3).

SSN model improvements varied with the solute of concern and network position. For Na^+, the SSN model reduced the AIC by 61%, RMSPE by 20%, and unexplained variance by 96% compared to the MLR model (Table 4). In contrast, the NO_3^- SSN model only reduced the AIC by <1%, the RMSPE by 7%, and the unexplained variance by 54% (Table 4). SSN model improvements tend to be smaller where spatial autocorrelation is lower (Isaak et al., 2014) such as with NO_3^- at our sites. Additionally, SSN models improved predictions more in downstream positions whereas MLR prediction error was relatively consistent across network positions (Figure 4C-D). Moving downstream, SSN models are informed by an increasing number of upstream data points. Conversely, SSN predictions in headwater locations rely more on watershed attributes than upstream data, much like MLR models.

4.2 Post-fire vegetation is a dominant driver of stream NO_3^- patterns

Large high severity fire has the potential to shift ecosystems from forest to grass and shrubland which can have implications for watershed N cycling. Even decades after the Hayman and nearby fires, 75% of high severity plots had no conifer regeneration and it is possible that forest density will never return to pre-fire levels in these areas (Chambers et al., 2016). Beyond our field sites, there is broad evidence of declining post-fire tree regeneration due to increasing climate aridity and fire activity which can shift previously forested systems into alternative stable states dominated by grassland and weedy, herbaceous vegetation types (Coop et al., 2020; Stevens-Rumann et al., 2018; Tepley et al., 2017; Walker et al., 2018). Forest cover is often a primary mechanism for terrestrial N retention (Dunnette et al., 2014; Vitousek et al., 1979) and changes from forest to grass and shrub cover can impact ecosystem N retention (Lovett et al., 2002). For example, conifers will more strongly regulate N cycling than grasses and forbs given their underlying nutrient use efficiencies (Chapman et al., 2006). Therefore, post-fire watersheds with little tree regeneration will likely be leakier with respect to N cycling.

Spectral vegetation indices were the strongest predictors of stream NO_3^- in this and other studies. For example, reduced post-fire plant cover, measured as NDVI, explained the persistence of elevated post-fire stream N (Rust et al., 2019). In this study though, the strongest predictor of stream NO_3^- concentration was mean NDMI (Table 3), a vegetation index that considers both canopy cover and the water stress of that vegetation. NDMI is more sensitive to burn severity, forest type, and forest loss and recovery than NDVI which is broadly sensitive to the amount of photosynthetically active vegetation (Morresi et al., 2019). The strong inverse relationship between NDMI and stream NO_3^- demonstrates that vegetation cover was a primary control on watershed N retention across spatial scales and the loss of forest cover lead to elevated stream NO_3^-. This is consistent with earlier work demonstrating that stream NO_3^-concentrations were inversely related to riparian vegetation exposure (Rhoades et al., 2019).

Rapid in-stream uptake and processing contribute to variability in stream NO_3^- concentrations (Bernhardt et al., 2003). Nitrate uptake lengths in nearby Wyoming streams ranged from hundreds to thousands of meters (Hall et al., 2009), so uptake is likely to influence NO_3^- patterns across the range of scales in our study (<9,000 m). However, headwater streams with elevated ambient inorganic N concentrations have a limited ability to moderate downstream transport of inorganic N (Covino et al., 2021b) because nutrient delivery to streams is often orders of magnitude greater than in-stream production or removal (Brookshire et al., 2009). Our previous work at the Hayman Fire demonstrated that in-stream biotic N demand increased after the fire, but N supply from burned uplands exceeded the increase in stream N demand (Rhea et al., 2021). While in-stream uptake likely contributed to spatial variability in stream NO_3^-, our work demonstrates strong post-fire vegetation controls on the spatial patterns of stream NO_3^-concentrations.

4.3 Burned headwaters are susceptible to elevated stream NO_3^-

Patterns of vegetation cover interact with watershed structure to drive spatial distributions of stream NO_3^-concentrations. Terrestrial inputs of water and dissolved solutes comprise a large portion of streamwater composition in headwater positions, making these areas particularly sensitive to disturbance in the surrounding uplands (Gomi et al., 2002; Likens & Bormann, 1974; Lowe & Likens, 2005). Thus, the vegetation cover of large convergent hillslopes should have stronger proportional influence on stream NO_3^- concentration in headwater positions relative to locations lower in the network. We found that convergent hillslopes in the headwaters of Brush Creek were associated with low NDMI (Figure 5E) and aligned with locations of high stream NO_3^- (Figure 5E). Proportional inflows declined downstream and were associated with higher NDMI. Stream NO_3^- also declined downstream in Brush Creek, likely due to a combination of reduced proportional influence of hillslope inputs, streamflow dilution, and in-stream N uptake. In the unburned headwaters of Pine Creek, convergent hillslopes were associated with high NDMI (Figure 5F) and likely high terrestrial N demand. Stream NO_3^-concentrations remained low throughout the headwaters with only slight downstream increases where hillslopes were sparsely vegetated (Figure 5F).

This investigation demonstrates that convergent hillslopes in headwater positions are particularly sensitive to wildfire-induced vegetation mortality and can impact both local and downstream water quality. Headwater attributes have been shown to predict downstream water chemistry (i.e., NO_3^-, PO_4^{3-}, Ca^{2+}, and Sr^{2+}) at distances > 500 km (French et al., 2020). The sampled stream networks were only 5,520 - 8,289 m, so headwater attributes could feasibly influence downstream chemistry throughout the entire stream networks. Indeed, the watershed with burned headwaters (i.e., Brush), sustained higher stream NO_3^- concentrations throughout its stream network compared to the watershed with unburned headwaters (i.e., Pine, Figure 5E-F). These findings may help prioritize post-fire watershed rehabilitation efforts aimed at increasing plant cover and nutrient demand to reduce stream NO_3^-concentrations. More specifically, our findings highlight the potential value for post-fire regeneration in convergent headwater locations to enhance N retention and reduce downstream NO_3^- export.

5 Conclusions

This study utilized spatially distributed stream solute sampling to identify the controls on stream Na^+ and NO_3^- concentrations across a gradient of burn patterns. Statistical modeling was used to partition the variance in stream Na^+ and NO_3^- among landscape (i.e., topographic, vegetation, and fire predictors) and stream network (i.e., flow-connected distance) characteristics. Topographic, vegetation, and fire variables were poor predictors of stream Na^+whereas mean NDMI was the strongest predictor of stream NO_3^-. Strong positive spatial autocorrelation indicated that downstream hydrologic transport was the primary driver of spatially distributed Na^+concentrations. Conversely, stream NO_3^- exhibited high spatial variability and weak spatial structure across all spatial scales. These results suggest that complex wildfire patterns that create a mosaic of unburned forest interspersed with patches of shrubs and grasses can result in high variability in stream NO_3^- concentrations. We also found that sparse forest cover in severely burned convergent hillslopes in headwater positions had a disproportionate impact on stream NO_3^- concentrations, suggesting that targeted reforestation in these locations may help limit stream NO_3^- concentrations and downstream export.

6 Acknowledgments and Data

We are grateful for financial support from the US Forest Service National Fire Plan (2016-2019) and the Joint Fire Sciences Program (JFSP# 14-1-06-11). AR was supported by NASA Headquarters under the NASA Earth and Space Science Fellowship Program. Sincere thanks to Tim Fegel of the Rocky Mountain Research Station for his critical contributions to field and laboratory work. The authors declare no conflicts of interest. The data used in this paper are publicly available through CUASHI HydroShare: Rhea, A. (2022). Use of geostatistical models to evaluate landscape and stream network controls on post-fire stream nitrate concentrations, *HydroShare* , http://www.hydroshare.org/resource/e35a308d4672419c9f75f6897c823c92.

References

Abatzoglou, J. T., Kolden, C. A., Williams, A. P., Lutz, J. A., & Smith, A. M. S. (2017). Climatic influences on interannual variability in regional burn severity across western US forests. *International Journal of Wildland Fire* , *26* (4), 269–275. https://doi.org/10.1071/WF16165

Abbott, B. W., Gruau, G., Zarnetske, J. P., Moatar, F., Barbe, L., Thomas, Z., et al. (2018). Unexpected spatial stability of water chemistry in headwater stream networks. *Ecology Letters* ,*21* (2), 296–308.

https://doi.org/10.1111/ele.12897

Abbott, B. W., Rocha, A. V., Shogren, A., Zarnetske, J. P., Iannucci, F., Bowden, W. B., et al. (2021). Tundra wildfire triggers sustained lateral nutrient loss in Alaskan Arctic. *Global Change Biology* ,*27* (7), 1408–1430. https://doi.org/10.1111/gcb.15507

Alexander, R. B., Boyer, E. W., Smith, R. A., Schwarz, G. E., & Moore, R. B. (2007). The role of headwater streams in downstream water quality.*Journal of the American Water Resources Association* ,*43* (1), 41–59. https://doi.org/10.1111/j.1752-1688.2007.00005.x

Allred, B. W., Bestelmeyer, B. T., Boyd, C. S., Brown, C., Davies, K. W., Duniway, M. C., et al. (2021). Improving Landsat predictions of rangeland fractional cover with multitask learning and uncertainty.*Methods in Ecology and Evolution* , *2021* (January), 1–9. https://doi.org/10.1111/2041-210x.13564

Baiamonte, G., & Singh, V. P. (2016). Overland Flow Times of Concentration for Hillslopes of Complex Topography. *Journal of Irrigation and Drainage Engineering* , *142* (3), 04015059. https://doi.org/10.1061/(asce)ir.1943-4774.0000984

Bergstrom, A., McGlynn, B., Mallard, J., & Covino, T. (2016). Watershed structural influences on the distributions of stream network water and solute travel times under baseflow conditions. *Hydrological Processes* , *30* (15), 2671–2685. https://doi.org/10.1002/hyp.10792

Bernhardt, E. S., Likens, G. E., Buso, D. C., & Driscoll, C. T. (2003). In-stream uptake dampens effects of major forest disturbance on watershed nitrogen export. *Proceedings of the National Academy of Sciences of the United States of America* , *100* (18), 10304–10308. https://doi.org/10.1073/pnas.1233676100

Bernhardt, E. S., Likens, G. E., Hall, R. O., Buso, D. C., Fisher, S. G., Burton, T. M., et al. (2005). Can't See the Forest for the Stream? In-stream Processing and Terrestrial Nitrogen Exports.*BioScience* , *55* (3), 219–230. https://doi.org/10.1641/0006-3568(2005)055[0219:acstff]2.0.co;2

Brennan, S. R., Torgersen, C. E., Hollenbeck, J. P., Fernandez, D. P., Jensen, C. K., & Schindler, D. E. (2016). Dendritic network models: Improving isoscapes and quantifying influence of landscape and in-stream processes on strontium isotopes in rivers. *Geophysical Research Letters* , *43* (10), 5043–5051. https://doi.org/10.1002/2016GL068904

Brookshire, E. N. J., Valett, H. M., & Gerber, S. (2009). Maintenance of terrestrial nutrient loss signatures during in-stream transport.*Ecology* , *90* (2), 293–299.

Brown, T. C., Hobbins, M. T., & Ramirez, J. A. (2008). Spatial distribution of water supply in the coterminous United States.*Journal of the American Water Resources Association* ,*44* (6), 1474–1487. https://doi.org/10.1111/j.1752-1688.2008.00252.x

Chambers, M. E., Fornwalt, P. J., Malone, S. L., & Battaglia, M. A. (2016). Patterns of conifer regeneration following high severity wildfire in ponderosa pine – dominated forests of the Colorado Front Range. *Forest Ecology and Management* , *378* , 57–67. https://doi.org/10.1016/j.foreco.2016.07.001

Chapin, F. S., Mooney, H. A., & Matson, P. A. (2011). *Principles of Terrestrial Ecosystem Ecology* (2nd ed.). New York, NY: Springer.

Chapman, S. K., Langley, J. A., Hart, S. C., & Koch, G. W. (2006). Plants actively control nitrogen cycling: Uncorking the microbial bottleneck. *New Phytologist* , *169* (1), 27–34. https://doi.org/10.1111/j.1469-8137.2005.01571.x

Cho, J. H., & Lee, J. H. (2018). Multiple linear regression models for predicting nonpoint-source pollutant discharge from a highland agricultural region. *Water (Switzerland)* , *10* (9). https://doi.org/10.3390/w10091156

Cipra, J., Kelly, E., MacDonald, L., & Norman, J. (2003). Soil properties, erosion, and implications for rehabilitation and aquatic ecosystems. *Hayman Fire Case Study* , 204–219.

Coop, J. D., Parks, S. A., Stevens-Rumann, C. S., Crausbay, S. D., Higuera, P. E., Hurteau, M. D., et al. (2020). Wildfire-Driven Forest Conversion in Western North American Landscapes. *BioScience* ,*70* (8), 659–673. https://doi.org/10.1093/biosci/biaa061

Cooper, S. D., Barmuta, L., Sarnelle, O., Kratz, K., & Diehl, S. (1997). Quantifying spatial heterogeneity in streams. *Journal of the North American Benthological Society* , *16* (1), 174–188. https://doi.org/10.2307/1468250

Covino, T., Riveros-Iregui, D. A., & Schneider, C. L. (2021).*Geomorphology Imparts Spatial Organization on Hydrological and Biogeochemical Fluxes* . *Reference Module in Earth Systems and Environmental Sciences* . Elsevier Inc. https://doi.org/10.1016/b978-0-12-818234-5.00068-7

Covino, T. P., Wlostowski, A. N., Gooseff, M. N., Wollheim, W. M., & Bowden, W. B. (2021). The Seasonality of In-Stream Nutrient Concentrations and Uptake in Arctic Headwater Streams in the Northern Foothills of Alaska's Brooks Range. *Journal of Geophysical Research: Biogeosciences* , *126* (4), 1–18. https://doi.org/10.1029/2020JG005949

Creed, I. F., & Beall, F. D. (2009). Distributed topographic indicators for predicting nitrogen export from headwater catchments. *Water Resources Research* , *45* (10). https://doi.org/10.1029/2008WR007285

Detty, J. M., & McGuire, K. J. (2010). Topographic controls on shallow groundwater dynamics: Implications of hydrologic connectivity between hillslopes and riparian zones in a till mantled catchment.*Hydrological Processes* , *24* (16), 2222–2236. https://doi.org/10.1002/hyp.7656

Dingman, L. S. (2015). *Physical Hydrology* (3rd ed.). Long Grove, IL: Waveland Press, Inc.

Dunnette, P. V., Higuera, P. E., Mclauchlan, K. K., Derr, K. M., Briles, C. E., & Keefe, M. H. (2014). Biogeochemical impacts of wildfires over four millennia in a Rocky Mountain subalpine watershed. *New Phytologist* , *203* (3), 900–912. https://doi.org/10.1111/nph.12828

Eidenshink, J., Schwind, B., Brewer, K., Zhu, Z.-L., Quayle, B., & Howard, S. (2009). A Project for Monitoring Trends in Burn Severity.*Fire Ecology* , *3* (1), 3–21. https://doi.org/10.4996/fireecology.0301003

French, D. W., Schindler, D. E., Brennan, S. R., & Whited, D. (2020). Headwater Catchments Govern Biogeochemistry in America's Largest Free-Flowing River Network. *Journal of Geophysical Research: Biogeosciences* , *125* (12), 1–20. https://doi.org/10.1029/2020JG005851

Ganio, L. M., Torgersen, C. E., & Gresswell, R. E. (2005). A geostatistical approach for describing spatial pattern in stream networks. *Frontiers in Ecology and the Environment* , *3* (3), 138–144.

Gomi, T., Sidle, R. C., & Richardson, J. S. (2002). Understanding processes and downstream linkages of headwater systems.*BioScience* , *52* (10), 905–916. https://doi.org/10.1641/0006-3568(2002)052[0905:UPADLO]2.0.CO;2

Graham, R. T. (2003). *Hayman Fire Case Study* . *Gen. Tech. Rep. RMRS- GTR-114* . Ogden, UT. Retrieved from http://www.fs.fed.us/rm/hayman_fire/

Hall, R. O., Sobota, D. J., Dodds, W. K., Findlay, S. E. G., Grimm, N. B., Hamilton, S. K., et al. (2009). Nitrate removal in stream ecosystems measured by 15N addition experiments: Denitrification. *Limnology and Oceanography* , *54* (3), 666–680. https://doi.org/10.4319/lo.2009.54.3.0666

Hall, S. (2017). The Legacy of Colorado's Largest Wildfire. *Denver Water* .

Hesselbarth, M., Sciaini, M., With, K., Wiegand, K., & Nowosad, J. (2019). landscapemetrics: an open-source R tool to calculate landscape metrics. *Ecography* , *42* , 1648–1657.

Ver Hoef, J. M., Peterson, E. E., Cliord, D., & Shah, R. (2014). Ssn: An R package for spatial statistical modeling on stream networks.*Journal of Statistical Software* , *56* (3), 1–45. https://doi.org/10.18637/jss.v056.i03

Ver Hoef, J., & Peterson, E. (2020). SSN. R package version 1.1.15. Retrieved from https://cran.r-project.org/web/packages/SSN/SSN.pdf

Huntington, J. L., Hegewisch, K. C., Daudert, B., Morton, C. G., Abatzoglou, J. T., McEvoy, D. J., & Erickson, T. (2017). Climate engine: Cloud computing and visualization of climate and remote sensing data for advanced natural resource monitoring and process understanding.*Bulletin of the American Meteorological Society* , *98* (11), 2397–2409. https://doi.org/10.1175/BAMS-D-15-00324.1

Isaak, D. J., Peterson, E. E., Ver Hoef, J. M., Wenger, S. J., Falke, J. A., Torgersen, C. E., et al. (2014). Applications of spatial statistical network models to stream data. *Wiley Interdisciplinary Reviews: Water* , *1* (3), 277–294. https://doi.org/10.1002/wat2.1023

Jencso, K. G., McGlynn, B. L., Gooseff, M. N., Bencala, K. E., & Wondzell, S. M. (2010). Hillslope hydrologic connectivity controls riparian groundwater turnover: Implications of catchment structure for riparian buffering and stream water sources. *Water Resources Research* , *46* (10), 1–18. https://doi.org/10.1029/2009WR008818

Kattwinkel, M., & Szöcs, E. (2020). openSTARS: An Open Source Implementation of the “ArcGIS” Toolbox “STARS”. R package version 1.2.2. Retrieved from https://cran.r-project.org/package=openSTARS

Lentile, L. B., Morgan, P., Hudak, A. T., Bobbitt, M. ., Lewis, S. A., Smith, A. M. S., & Robichaud, P. R. (2007). Post-fire burn severity and vegetation response following eight large wildfires across the Western United States. *Fire Ecology* , *3* (1), 91–108. https://doi.org/10.1227/01.NEU.0000089482.80879.9A

Likens, G. E., & Bormann, F. H. (1974). Linkages between Terrestrial and Aquatic Ecosystems. *BioScience* , *24* (8), 447–456. https://doi.org/10.2307/1296852

Likens, G. E., Bormann, F. H., Johnson, N. M., Fisher, D. W., & Pierce, R. S. (1970). Effects of Forest Cutting and Herbicide Treatment on Nutrient Budgets in the Hubbard Brook Watershed-Ecosystem.*Ecological Monographs* , *40* (1), 23–47. https://doi.org/10.2307/1942440

Lindsay, J. B. (2020). WhiteboxTools Version 1.4.0. Guelpg, Canada.

Lovett, G. M., Weathers, K. C., & Arthur, M. A. (2002). Control of nitrogen loss from forested watersheds by soil carbon:Nitrogen ratio and tree species composition. *Ecosystems* , *5* (7), 712–718. https://doi.org/10.1007/s10021-002-0153-1

Lowe, W. H., & Likens, G. E. (2005). Moving Headwater Streams to the Head of the Class. *BioScience* , *55* (3), 196–197. Retrieved from https://doi.org/10.1641/0006-3568(2005)055[0196:MHSTTH]2.0.CO;2

Mallard, J., McGlynn, B., & Covino, T. (2014). Lateral inflows, stream-groundwater exchange, and network geometry influence stream water composition. *Water Resources Research* , *50* , 4603–4623. https://doi.org/10.1002/2013WR014979.Reply

McGuire, K. J., Torgersen, C. E., Likens, G. E., Buso, D. C., Lowe, W. H., & Bailey, S. W. (2014). Network analysis reveals multiscale controls on streamwater chemistry. *Proceedings of the National Academy of Sciences of the United States of America* , *111* (19), 7030–7035. https://doi.org/10.1073/pnas.1404820111

McManus, M. G., D’amico, E., Smith, E. M., Polinsky, R., Ackerman, J., & Tyler, K. (2020). Variation in stream network relationships and geospatial predictions of watershed conductivity. *Freshwater Science* , *39* (4), 704–721. https://doi.org/10.1086/710340

Morresi, D., Vitali, A., Urbinati, C., & Garbarino, M. (2019). Forest spectral recovery and regeneration dynamics in stand-replacing wildfires of central Apennines derived from Landsat time series. *Remote Sensing* , *11* (3). https://doi.org/10.3390/rs11030308

Parsons, A., Robichaud, P. R., Lewis, S. A., Napper, C., & Clark, J. T. (2010). *Field guide for mapping post-fire soil burn severity .Gen. Tech. Rep. RMRS-GTR-243* . Fort Collins, CO. https://doi.org/10.2737/RMRS-GTR-243

Peterson, E. E., & Ver Hoef, J. M. (2010). A mixed-model moving-average approach to geostatistical modeling in stream networks. *Ecology* ,*91* (3), 644–651.

Peterson, E. E., & Ver Hoef, J. M. (2014). STARS: An ArcGIS toolset used to calculate the spatial information needed to fit spatial statistical models to stream network data. *Journal of Statistical Software* , *56* , 1–17.

Rhea, A. E., Covino, T. P., & Rhoades, C. C. (2021). Reduced N-Limitation and Increased In-Stream Productivity of Autotrophic Biofilms 5 and 15 Years After Severe Wildfire. *Journal of Geophysical Research: Biogeosciences* , *126* (9), 1–16. https://doi.org/10.1029/2020JG006095

Rhoades, C. C., Entwistle, D., & Butler, D. (2011). The influence of wildfire extent and severity on streamwater chemistry, sediment and temperature following the Hayman Fire, Colorado. *International Journal of Wildland Fire* , *20* (3), 430–442. https://doi.org/10.1071/WF09086

Rhoades, C. C., Chow, A. T., Covino, T. P., Fegel, T. S., Pierson, D. N., & Rhea, A. E. (2019). The Legacy of a Severe Wildfire on Stream Nitrogen and Carbon in Headwater Catchments. *Ecosystems* ,*22* (3), 643–657. https://doi.org/10.1007/s10021-018-0293-6

Richer, E. E., Kampf, S. K., Fassnacht, S. R., & Moore, C. C. (2013). Spatiotemporal index for analyzing controls on snow climatology: Application in the Colorado Front Range. *Physical Geography* ,*34* (2), 85–107. https://doi.org/10.1080/02723646.2013.787578

Robichaud, P., MacDonald, L., Freeouf, J., Neary, D., Martin, D., & Ashmun, L. (2003). Postfire Rehabilitation of the Hayman Fire.*Hayman Fire Case Study: USDA RMRS-GTR-114* , 293–313. Retrieved from http://www.fs.fed.us/rm/pubs/rmrs_gtr114/rmrs_gtr114_293_314.pdf

Rodríguez-González, P. M., García, C., Albuquerque, A., Monteiro-Henriques, T., Faria, C., Guimarães, J. B., et al. (2019). A spatial stream-network approach assists in managing the remnant genetic diversity of riparian forests. *Scientific Reports* , *9* (1), 1–10. https://doi.org/10.1038/s41598-019-43132-7

Ruleman, C. A., Bohannon, R. G., Bryant, Bruce, Shroba, R. R., & Premo, W. R. (2011). Geologic map of the Bailey 30' x 60' quadrangle, north-central Colorado: U.S. Geological Survey, Scientific Investigations Map SIM-3156, scale 1:100,000.

Rust, A. J., Hogue, T. S., Saxe, S., & McCray, J. (2018). Post-fire water-quality response in the western United States. *International Journal of Wildland Fire* , *27* (3), 203–216. https://doi.org/10.1071/WF17115

Rust, A. J., Saxe, S., McCray, J., Rhoades, C. C., & Hogue, T. S. (2019). Evaluating the factors responsible for post-fire water quality response in forests of the western USA. *International Journal of Wildland Fire* , *28* (10), 769–784. https://doi.org/10.1071/WF18191

Seibert, J., & McGlynn, B. L. (2007). A new triangular multiple flow direction algorithm for computing upslope areas from gridded digital elevation models. *Water Resources Research* , *43* (4), 1–8. https://doi.org/10.1029/2006WR005128

Shogren, A. J., Zarnetske, J. P., Abbott, B. W., Iannucci, F., Medvedeff, A., Cairns, S., et al. (2021). Arctic concentration–discharge relationships for dissolved organic carbon and nitrate vary with landscape and season. *Limnology and Oceanography* , *66* (S1), S197–S215. https://doi.org/10.1002/lno.11682

Smith, H. G., Sheridan, G. J., Lane, P. N. J., Nyman, P., & Haydon, S. (2011). Wildfire effects on water quality in forest catchments: A review with implications for water supply. *Journal of Hydrology* ,*396* (1–2), 170–192. https://doi.org/10.1016/j.jhydrol.2010.10.043

Smithwick, E. A. H., Kashian, D. M., Ryan, M. G., & Turner, M. G. (2009). Long-term nitrogen storage and soil nitrogen availability in post-fire lodgepole pine ecosystems. *Ecosystems* , *12* (5), 792–806. https://doi.org/10.1007/s10021-009-9257-1

Stevens-Rumann, C. S., Kemp, K. B., Higuera, P. E., Harvey, B. J., Rother, M. T., Donato, D. C., et al. (2018). Evidence for declining forest resilience to wildfires under climate change. *Ecology Letters* , *21* (2), 243–252. https://doi.org/10.1111/ele.12889

Stream Solute Workshop. (1990). Concepts and Methods for Assessing Solute Dynamics in Stream Ecosystems. *Journal of the North American Benthological Society* , *9* (2), 95–119. https://doi.org/10.2307/1467445

Taylor, A. H., Poulos, H. M., Kluber, J., Issacs, R., Pawlikowski, N., & Barton, A. M. (2021). Controls on spatial patterns of wildfire severity and early post-fire vegetation development in an Arizona Sky Island, USA. *Landscape Ecology* , *36* (9), 2637–2656. https://doi.org/10.1007/s10980-021-01260-4

Tepley, A. J., Thompson, J. R., Epstein, H. E., & Anderson-Teixeira, K. J. (2017). Vulnerability to forest loss through altered postfire recovery dynamics in a warming climate in the Klamath Mountains. *Global Change Biology* , *23* (10), 4117–4132. https://doi.org/10.1111/gcb.13704

Turner, M. G., Smithwick, E. A. H., Metzger, K. L., Tinker, D. B., & Romme, W. H. (2007). Inorganic nitrogen availability after severe stand-replacing fire in the Greater Yellowstone ecosystem. *Proceedings of the National Academy of Sciences of the United States of America* , *104* (12), 4782–4789. https://doi.org/10.1073/pnas.0700180104

U.S. Geological Survey. (2018). 3D Elevation Program 10-Meter Resolution Digital Elevation Model. Retrieved from https://www.usgs.gov/core-science-systems/ngp/3dep/data-tools

Vannote, R., Minshall, G., Cummins, K., Sedell, J., & Cushing, C. (1980). The River Continuum Concept. *Canadian Journal of Fisheries and Aquatic Sciences* , *37* , 130–137.

Vitousek, P. M., Gosz, J. R., Grier, C. C., Melillo, J. M., William, A., & Todd, R. L. (1979). Nitrate Losses from Disturbed Ecosystems. *Science* , *204* (4392), 469–474.

Walker, R. B., Coop, J. D., Parks, S. A., & Trader, L. (2018). Fire regimes approaching historic norms reduce wildfire-facilitated conversion from forest to non-forest. *Ecosphere* , *9* (4). https://doi.org/10.1002/ecs2.2182

Wan, S., Hui, D., & Luo, Y. (2001). Fire effects on nitrogen pools and dynamics in terrestrial ecosystems: A meta-analysis. *Ecological Applications* , *11* (5), 1349–1365. https://doi.org/10.1890/1051-0761(2001)011[1349:FEONPA]2.0.CO;2

Webster, J. R., & Valett, H. M. (2006). Solute Dynamics. In *Methods in Stream Ecology* (2nd ed., pp. 169–185). Elsevier.

Westerling, A. L. R. (2016). Increasing western US forest wildfire activity: Sensitivity to changes in the timing of spring. *Philosophical Transactions of the Royal Society B: Biological Sciences* , *371* (1696). https://doi.org/10.1098/rstb.2015.0178

Wilson, C., Kampf, S. K., Wagenbrenner, J. W., & MacDonald, L. H. (2018). Rainfall thresholds for post-fire runoff and sediment delivery from plot to watershed scales. *Forest Ecology and Management* , *430* (August), 346–356. https://doi.org/10.1016/j.foreco.2018.08.025

Wohl, E. (2017). The significance of small streams. *Frontiers of Earth Science* , *11* (3), 447–456. https://doi.org/10.1007/s11707-017-0647-y

WRCC. (2021). Daily Total Precipitation Cheesman, Colorado (Station 053102). Retrieved from https://wrcc.dri.edu/cgi-bin/rawMAIN.pl?coCCHE

Wu, Q. (2021). whitebox: "WhiteboxTools" R Frontend. R package version 1.4.0. Retrieved from https://github.com/giswqs/whiteboxR

Zarnetske, J. P., Bouda, M., Abbott, B. W., Saiers, J., & Raymond, P. A. (2018). Generality of Hydrologic Transport Limitation of Watershed Organic Carbon Flux Across Ecoregions of the United States. *Geophysical Research Letters* , *45* (21), 11,702-11,711. https://doi.org/10.1029/2018GL080005